

Light meson spectroscopy and gluonium searches in η_c and $\Upsilon(1S)$ decays at BaBar

Antimo Palano,
INFN Sezione di Bari, Italy

Abstract

We study the $\Upsilon(1S)$ radiative decays to $\gamma\pi^+\pi^-$ and γK^+K^- using data recorded with the BaBar detector operating at the SLAC PEP-II asymmetric-energy e^+e^- collider at center-of-mass energies at the $\Upsilon(2S)$ and $\Upsilon(3S)$ resonances. The $\Upsilon(1S)$ resonance is reconstructed from the decay $\Upsilon(nS) \rightarrow \pi^+\pi^-\Upsilon(1S)$, $n = 2, 3$. We also study the processes $\gamma\gamma \rightarrow \eta_c \rightarrow \eta' K^+K^-$, $\eta'\pi^+\pi^-$, and $\eta\pi^+\pi^-$ using a data sample of 519 fb^{-1} recorded with the BaBar detector at center-of-mass energies at and near the $\Upsilon(nS)$ ($n = 2, 3, 4$) resonances. A Dalitz plot analysis is performed of η_c decays to $\eta' K^+K^-$, $\eta'\pi^+\pi^-$, and $\eta\pi^+\pi^-$. A new $a_0(1700)$ resonance is observed in the $\eta\pi^\pm$ invariant-mass spectrum from the $\eta_c \rightarrow \eta\pi^+\pi^-$ decay. We compare η_c decays to η and η' final states in association with scalar mesons as they relate to the identification of the scalar glueball.

On behalf of the BaBar Collaboration
Presented at the “Eighth Workshop on Theory, Phenomenology and Experiments in Flavour Physics”-FPCapri2022

Jun 11 – 13, 2022, Villa Orlandi, Anacapri, Capri Island, Italy

1 Introduction

The existence of gluonium states is still an open issue for Quantum Chromodynamics (QCD). Lattice QCD calculations predict the lightest gluonium states to have quantum numbers $J^{PC} = 0^{++}$ and 2^{++} and to be in the mass region below 2.5 GeV/ c^2 [1]. In particular, the $J^{PC} = 0^{++}$ glueball is predicted to have a mass around 1.7 GeV/ c^2 . The broad $f_0(500)$, $f_0(1370)$ [2], $f_0(1500)$ [3, 4], $f_0(1710)$ [5, 6] and possibly the $f_0(2100)$ [7] have been suggested as scalar glueball candidates. However, the identification of the scalar glueball is complicated by the possible mixing with standard $q\bar{q}$ states.

Radiative decays of heavy quarkonia, in which a photon replaces one of the three gluons from the strong decay of J/ψ or $\Upsilon(1S)$, can probe color-singlet two-gluon systems that produce gluonic resonances. J/ψ decays have been extensively studied [8, 9]. In the first BaBar analysis [10] summarized in the present review, we study $\Upsilon(1S)$ decays, taking into account that the experimental observation of radiative $\Upsilon(1S)$ decays is challenging because their rate is suppressed by a factor of ≈ 0.025 compared to J/ψ radiative decays, which are of order 10^{-3} [11].

Decays of the η_c , the lightest pseudoscalar $c\bar{c}$ state, provide a window on light meson states. In the second analysis [12] summarized in the present review, we consider the three-body η_c decays to $\eta'K^+K^-$, $\eta'\pi^+\pi^-$, and $\eta\pi^+\pi^-$, using two-photon interactions, $e^+e^- \rightarrow e^+e^-\gamma^*\gamma^* \rightarrow e^+e^-\eta_c$. If both of the virtual photons are quasi-real, the allowed J^{PC} values of any produced resonances are $0^{\pm\pm}$, $2^{\pm\pm}$, $4^{\pm\pm}$... [13]. The possible presence of a gluonic component of the η' meson, due to the so-called gluon anomaly, has been discussed in recent years [14, 15]. A comparison of the η and η' content of η_c decays might yield information on the possible gluonic content of resonances decaying to $\pi^+\pi^-$ or K^+K^- .

2 Study of $\Upsilon(1S)$ radiative decays to $\gamma\pi^+\pi^-$ and γK^+K^-

2.1 Events reconstruction

We reconstruct the decay chains

$$\Upsilon(2S)/\Upsilon(3S) \rightarrow (\pi_s^+\pi_s^-)\Upsilon(1S) \rightarrow (\pi_s^+\pi_s^-)(\gamma\pi^+\pi^-) \quad (1)$$

and

$$\Upsilon(2S)/\Upsilon(3S) \rightarrow (\pi_s^+\pi_s^-)\Upsilon(1S) \rightarrow (\pi_s^+\pi_s^-)(\gamma K^+K^-), \quad (2)$$

where we label with the subscript s the slow pions from the direct $\Upsilon(2S)$ and $\Upsilon(3S)$ decays.

Events with balanced momentum are required to satisfy energy balance requirements. For each combination of $\pi_s^+\pi_s^-$ candidates, we first require both particles to be identified loosely as pions and compute the recoiling mass

$$M_{\text{rec}}^2(\pi_s^+\pi_s^-) = |p_{e^+} + p_{e^-} - p_{\pi_s^+} - p_{\pi_s^-}|^2, \quad (3)$$

where p is the particle four-momentum. The distribution of $M_{\text{rec}}^2(\pi_s^+\pi_s^-)$ is expected to peak at the squared $\Upsilon(1S)$ mass for signal events. Figure 1 shows the combinatorial recoiling mass $M_{\text{rec}}(\pi_s^+\pi_s^-)$ for $\Upsilon(2S)$ and $\Upsilon(3S)$ data, where narrow peaks at the $\Upsilon(1S)$ mass can be observed.

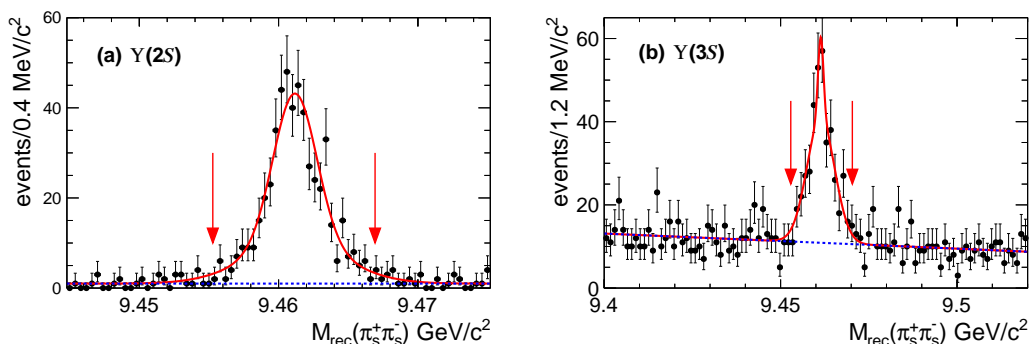


Figure 1: Combinatorial recoiling mass M_{rec} to $\pi_s^+ \pi_s^-$ candidates for (a) $\Upsilon(2S)$ and (b) $\Upsilon(3S)$ data. The arrows indicate the regions used to select the $\Upsilon(1S)$ signal.

We select signal event candidates by requiring

$$|M_{\text{rec}}(\pi_s^+ \pi_s^-) - m(\Upsilon(1S))_f| < 2.5\sigma, \quad (4)$$

where $m(\Upsilon(1S))_f$ indicates the fitted $\Upsilon(1S)$ mass value and $\sigma = 2.3 \text{ MeV}/c^2$ and $\sigma = 3.5 \text{ MeV}/c^2$ for $\Upsilon(2S)$ and $\Upsilon(3S)$ data, respectively. To reconstruct $\Upsilon(1S) \rightarrow \gamma \pi^+ \pi^-$ or $\Upsilon(1S) \rightarrow \gamma K^+ K^-$ decays, we require a loose identification of both pions or kaons and isolate the two $\Upsilon(1S)$ decay modes by requiring

$$9.1 \text{ GeV}/c^2 < m(\gamma h^+ h^-) < 9.6 \text{ GeV}/c^2, \quad (5)$$

where $h = \pi, K$.

2.2 Study of the $\pi^+ \pi^-$ and $K^+ K^-$ mass spectra

The $\pi^+ \pi^-$ mass spectrum, for $m(\pi^+ \pi^-) < 3.0 \text{ GeV}/c^2$ and summed over the $\Upsilon(2S)$ and $\Upsilon(3S)$ datasets with 507 and 277 events, respectively, is shown in Fig. 2(Left). The spectrum shows $I = 0, J^P = \text{even}^{++}$ resonance production, with low backgrounds above $1 \text{ GeV}/c^2$. We observe a rapid drop around $1 \text{ GeV}/c^2$ characteristic of the presence of the $f_0(980)$, and a strong $f_2(1270)$ signal. The data also suggest the presence of additional weaker resonant contributions.

The $K^+ K^-$ mass spectrum, summed over the $\Upsilon(2S)$ and $\Upsilon(3S)$ datasets with 164 and 63 events, respectively, is shown in Fig. 2(Right) and also shows resonant production, with low background. Signals at the positions of $f_2'(1525)/f_0(1500)$ and $f_0(1710)$ can be observed, with further unresolved structure at higher mass.

We make use of a phenomenological model to extract the different $\Upsilon(1S) \rightarrow \gamma R$ branching fractions, where R is an intermediate resonance. We perform a simultaneous binned fit to the $\pi^+ \pi^-$ mass spectra from the $\Upsilon(2S)$ and $\Upsilon(3S)$ datasets. We describe the low-mass region (around the $f_0(500)$) using a relativistic S -wave Breit-Wigner lineshape having free parameters. We describe the $f_0(980)$ using the Flatté [16] formalism with parameters fixed to the values from ref. [17]. The $f_2(1270)$ and $f_0(1710)$ resonances are represented by relativistic Breit-Wigner functions with parameters fixed to PDG values [18]. In the high $\pi^+ \pi^-$ mass region we include a

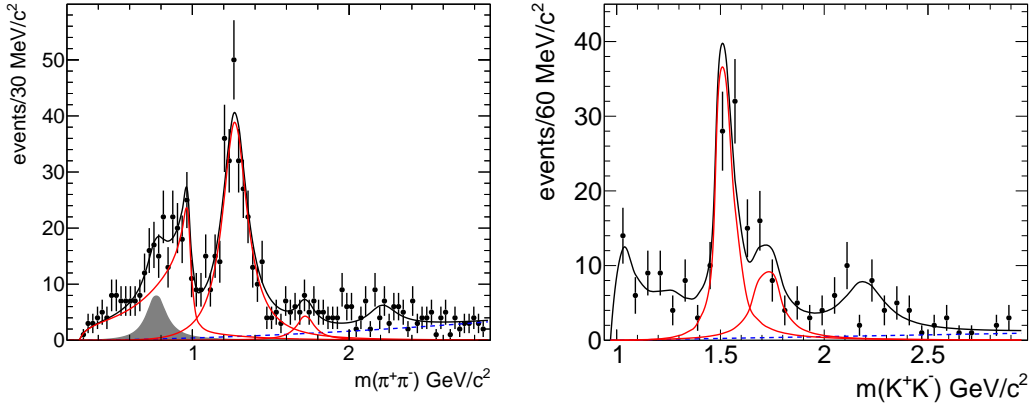


Figure 2: (Left) $\pi^+\pi^-$ mass distribution from $\Upsilon(1S) \rightarrow \pi^+\pi^-\gamma$ for the combined $\Upsilon(2S)$ and $\Upsilon(3S)$ datasets. The full (red) curves indicate the S -wave, $f_2(1270)$, and $f_0(1710)$ contributions. The shaded (gray) area represents the estimated $\rho(770)^0$ background. (Right) K^+K^- mass distribution from $\Upsilon(1S) \rightarrow K^+K^-\gamma$ for the combined $\Upsilon(2S)$ and $\Upsilon(3S)$ datasets. The (red) curves show the contributions from $f_2'(1525)/f_0(1500)$ and $f_0(1710)$. Dashed (blue) lines indicate the background contributions.

single resonance $f_0(2100)$ having a width fixed to the PDG value (224 ± 22) and unconstrained mass. For the $\Upsilon(3S)$ data we also include $\rho(770)^0$ background with parameters fixed to the PDG values. The fit is shown in Fig. 2. It has 16 free parameters and $\chi^2 = 182$ for $\text{ndf}=152$, corresponding to a p -value of 5%. We note the observation of a significant S -wave in $\Upsilon(1S)$ radiative decays. This observation was not possible in the study of J/ψ radiative decay to $\pi^+\pi^-$ because of the presence of a strong, irreducible background from $J/\psi \rightarrow \pi^+\pi^-\pi^0$ [19]. No evidence is found for a $\Upsilon(1S) \rightarrow \pi^+\pi^-\pi^0$ decay in present data. We obtain the following $f_0(500)$ parameters:

$$m(f_0(500)) = 0.856 \pm 0.086 \text{ GeV}/c^2, \Gamma(f_0(500)) = 1.279 \pm 0.324 \text{ GeV}, \quad (6)$$

and $\phi = 2.41 \pm 0.43$ rad. The fraction of S -wave events associated with the $f_0(500)$ is $(27.7 \pm 3.1)\%$.

We perform a binned fit to the combined K^+K^- mass spectrum using the following model. The $f_0(980)$ is parameterized according to the Flatté formalism. The $f_2(1270)$, $f_2'(1525)$, $f_0(1500)$, and $f_0(1710)$ resonances are represented by relativistic Breit-Wigner functions with parameters fixed to PDG values. We include an $f_0(2200)$ contribution having parameters fixed to the PDG values. The fit shown in Fig. 2(Right). It has six free parameters and $\chi^2 = 35$ for $\text{ndf}=29$, corresponding to a p -value of 20%. The resonances yields and significances are given in Table 1. Systematic uncertainties are dominated by the PDG uncertainties on resonances parameters.

The efficiency distributions as functions of mass, for the $\Upsilon(2S)/\Upsilon(3S)$ data and for the $\pi^+\pi^-\gamma$ and $K^+K^-\gamma$ final states, are found to have an almost uniform behavior for all the final states. We define the helicity angle θ_H as the angle formed by the h^+ , in the h^+h^- rest frame, and the γ in the $h^+h^-\gamma$ rest frame. We also define θ_γ as the angle formed by the radiative photon in the $h^+h^-\gamma$ rest frame with respect to the $\Upsilon(1S)$ direction in the $\Upsilon(2S)/\Upsilon(3S)$ rest frame. We

Table 1: Resonances yields and statistical significances from the fits to the $\pi^+\pi^-$ and K^+K^- mass spectra for the $\Upsilon(2S)$ and $\Upsilon(3S)$ datasets. The symbol $f_J(1500)$ indicates the signal in the 1500 MeV/ c^2 mass region.

Resonances ($\pi^+\pi^-$)	Yield $\Upsilon(2S)$	Yield $\Upsilon(3S)$	Significance
S -wave	$133 \pm 16 \pm 13$	87 ± 13	12.8σ
$f_2(1270)$	$255 \pm 19 \pm 8$	$77 \pm 7 \pm 4$	15.9σ
$f_0(1710)$	$24 \pm 8 \pm 6$	$6 \pm 8 \pm 3$	2.5σ
Resonances (K^+K^-)	Yield $\Upsilon(2S) + \Upsilon(3S)$		Significance
$f_0(980)$	47 ± 9		5.6σ
$f_J(1500)$	$77 \pm 10 \pm 10$		8.9σ
$f_0(1710)$	$36 \pm 9 \pm 6$		4.7σ

label with $\epsilon(m, \cos \theta_H)$ the efficiency computed as a function of the h^+h^- effective mass and the helicity angle $\cos \theta_H$. We label with $\epsilon(\cos \theta_H, \cos \theta_\gamma)$ the efficiency computed, for each resonance mass window, as a function of $\cos \theta_H$ and $\cos \theta_\gamma$. This is used to obtain the efficiency-corrected angular distributions and branching fractions for the different resonances. To obtain the efficiency correction weight w_R for the resonance R we divide each event by the efficiency $\epsilon(\cos \theta_H, \cos \theta_\gamma)$

$$w_R = \frac{\sum_{i=1}^{N_R} 1/\epsilon_i(\cos \theta_H, \cos \theta_\gamma)}{N_R}, \quad (7)$$

where N_R is the number of events in the resonance mass range.

2.3 Angular analysis

To obtain information on the angular momentum structure of the $\pi^+\pi^-$ and K^+K^- systems in $\Upsilon(1S) \rightarrow \gamma h^+h^-$ we study the dependence of the $m(h^+h^-)$ mass on the helicity angle θ_H . A better way to observe angular effects is to plot the $\pi^+\pi^-$ mass spectrum weighted by the Legendre polynomial moments, corrected for efficiency and shown in Fig. 3. In a simplified environment, the moments are related to the spin 0 (S) and spin 2 (D) amplitudes by the equations

$$\begin{aligned} \sqrt{4\pi}\langle Y_0^0 \rangle &= S^2 + D^2, \\ \sqrt{4\pi}\langle Y_2^0 \rangle &= 2SD \cos \phi_{SD} + 0.639D^2, \\ \sqrt{4\pi}\langle Y_4^0 \rangle &= 0.857D^2, \end{aligned} \quad (8)$$

where ϕ_{SD} is the relative phase. Therefore we expect to observe spin 2 resonances in $\langle Y_4^0 \rangle$ and S/D interference in $\langle Y_2^0 \rangle$. The results are shown in Fig. 3(Top). We clearly observe the $f_2(1270)$ resonance in $\langle Y_4^0 \rangle$ and a sharp drop in $\langle Y_2^0 \rangle$ at the $f_2(1270)$ mass, indicating the interference effect. The distribution of $\langle Y_0^0 \rangle$ is just the scaled $\pi^+\pi^-$ mass distribution, corrected

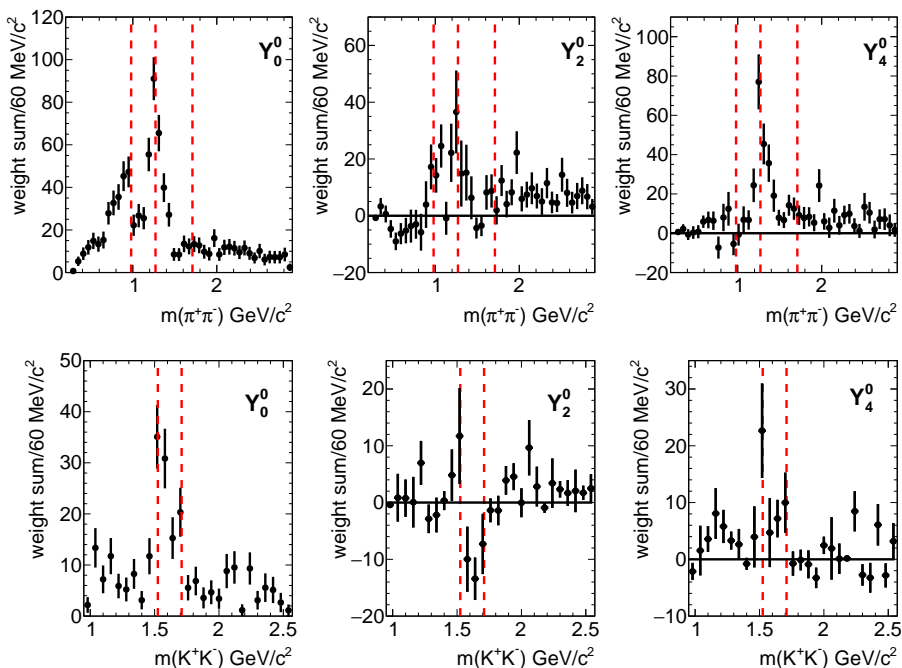


Figure 3: The distributions of the most relevant unnormalized Y_L^0 moments for $\Upsilon(1S) \rightarrow \gamma\pi^+\pi^-$ (Top) and $\Upsilon(1S) \rightarrow \gamma K^+K^-$ (Bottom) as functions of mass. The lines indicate the positions of $f_0(980)$, $f_2(1270)$, and $f_0(1710)$ for $\pi^+\pi^-$ and $f_2'(1525)$ and $f_0(1710)$ for K^+K^- .

for efficiency. Similarly, we plot in Fig. 3(Bottom) the K^+K^- mass spectrum weighted by the Legendre polynomial moments, corrected for efficiency. We observe signals of the $f_2'(1525)$ and $f_0(1710)$ in $\langle Y_4^0 \rangle$ and activity due to S/D interference effects in the $\langle Y_2^0 \rangle$ moment.

Resonance angular distributions in radiative $\Upsilon(1S)$ decays from $\Upsilon(2S)/\Upsilon(3S)$ decays are rather complex (see ref. [10] for details). Here we only perform a simplified Partial Wave Analysis (PWA) solving directly the system of Eq. (8). Figure 4 shows the resulting S -wave and D -wave contributions to the $\pi^+\pi^-$ and K^+K^- mass spectra, respectively. Due to the presence of background in the threshold region, the $\pi^+\pi^-$ analysis is performed only on the $\Upsilon(2S)$ data.

We note that in the case of the $\pi^+\pi^-$ mass spectrum we obtain a good separation between S and D -waves, with the presence of an $f_0(980)$ resonance on top of a broad $f_0(500)$ resonance in the S -wave and a clean $f_2(1270)$ in the D -wave distribution. Integrating the S -wave amplitude from threshold up to a mass of $1.5 \text{ GeV}/c^2$, we obtain an integrated, efficiency corrected yield $N(S\text{-wave}) = 629 \pm 128$.

In the case of the K^+K^- PWA the structure peaking around $1500 \text{ MeV}/c^2$ appears in both S and D -waves suggesting the presence of $f_0(1500)$ and $f_2'(1525)$. In the $f_0(1710)$ mass region there is not enough data to discriminate between the two different spin assignments. This pattern is similar to that observed in the Dalitz plot analysis of charmless $B \rightarrow 3K$ decays [20]. Integrating the S and D -wave contributions in the $f_2'(1525)/f_0(1500)$ mass region, we obtain a fraction of S -wave contribution $f_S(K^+K^-) = 0.53 \pm 0.10$.

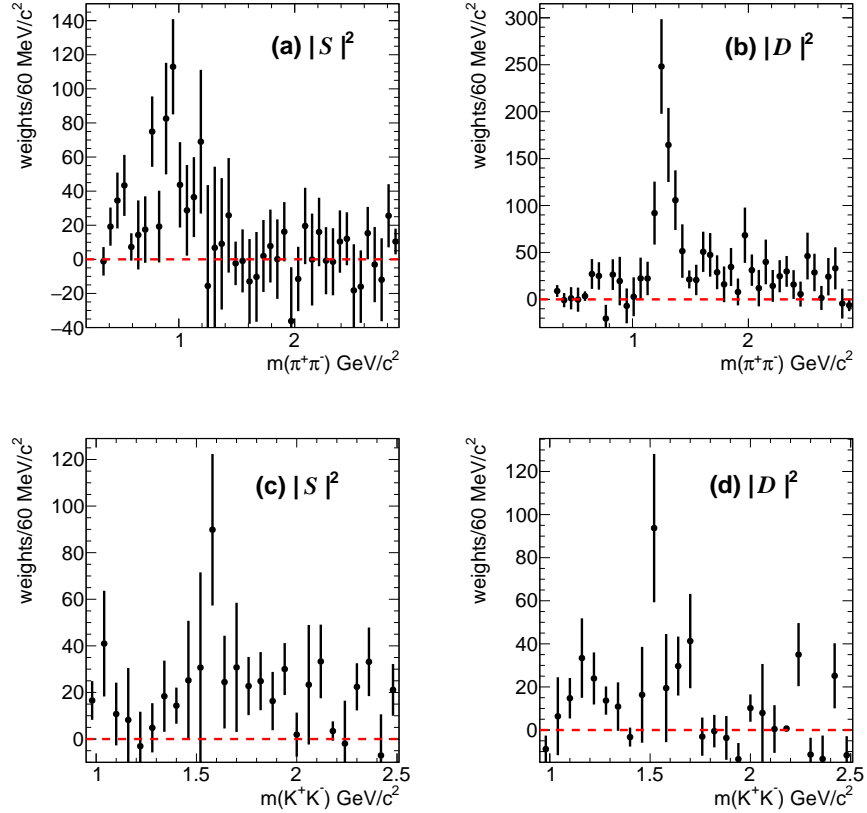


Figure 4: (a)-(c) S and (b)-(d) D -wave contributions from the simple PWA of the $\pi^+\pi^-$ mass spectrum for the $\Upsilon(2S)$ data (Left) and of the K^+K^- mass spectrum for the combined $\Upsilon(2S)/\Upsilon(3S)$ data (Right).

2.4 Measurement of branching fractions

We determine the branching fraction $\mathcal{B}(R)$ for the decay of $\Upsilon(1S)$ to photon and resonance R using the expression

$$\mathcal{B}(R) = \frac{N_R(\Upsilon(nS) \rightarrow \pi_s^+\pi_s^-\Upsilon(1S)(\rightarrow R\gamma))}{N(\Upsilon(nS) \rightarrow \pi_s^+\pi_s^-\Upsilon(1S)(\rightarrow \mu^+\mu^-))} \times \mathcal{B}(\Upsilon(1S) \rightarrow \mu^+\mu^-), \quad (9)$$

where N_R indicates the efficiency-corrected yield for the given resonance. To reduce systematic uncertainties, we first compute the relative branching fraction to the reference channel $\Upsilon(nS) \rightarrow \pi^+\pi^-\Upsilon(1S)(\rightarrow \mu^+\mu^-)$, which has the same number of charged particles as the final states under study. We then multiply the relative branching fraction by the well-measured branching fraction $\mathcal{B}(\Upsilon(1S) \rightarrow \mu^+\mu^-) = 2.48 \pm 0.05\%$ [18].

We determine the reference channel corrected yield using the method of “ B -counting”, also used to obtain the number of produced $\Upsilon(2S)$ and $\Upsilon(3S)$ [21]. Taking into account the known branching fractions of $\Upsilon(2S)/\Upsilon(3S) \rightarrow \pi_s^+\pi_s^-\Upsilon(1S)$ we obtain

$$N(\Upsilon(2S) \rightarrow \pi_s^+\pi_s^-\Upsilon(1S)(\rightarrow \mu^+\mu^-)) = (4.35 \pm 0.12_{\text{sys}}) \times 10^5 \quad (10)$$

and

$$N(\Upsilon(3S) \rightarrow \pi_s^+ \pi_s^- \Upsilon(1S) (\rightarrow \mu^+ \mu^-)) = (1.32 \pm 0.04_{\text{sys}}) \times 10^5 \quad (11)$$

events. Table 2 gives the measured branching fractions. In all cases we correct the efficiency corrected yields for isospin and for PDG measured branching fractions [18].

Table 2: Measured $\Upsilon(1S) \rightarrow \gamma R$ branching fractions.

Resonance	$\mathcal{B}(10^{-5})$
$\pi\pi$ <i>S</i> -wave	$4.63 \pm 0.56 \pm 0.48$
$f_2(1270)$	$10.15 \pm 0.59^{+0.54}_{-0.43}$
$f_0(1710) \rightarrow \pi\pi$	$0.79 \pm 0.26 \pm 0.17$
$f_J(1500) \rightarrow K\bar{K}$	$3.97 \pm 0.52 \pm 0.55$
$f_2'(1525)$	$2.13 \pm 0.28 \pm 0.72$
$f_0(1500) \rightarrow K\bar{K}$	$2.08 \pm 0.27 \pm 0.65$
$f_0(1710) \rightarrow K\bar{K}$	$2.02 \pm 0.51 \pm 0.35$

We report the first observation of $f_0(1710)$ in $\Upsilon(1S)$ radiative decay with a significance of 5.7σ , combining $\pi^+\pi^-$ and K^+K^- data. To determine the branching ratio of the $f_0(1710)$ decays to $\pi\pi$ and $K\bar{K}$, we remove all the systematic uncertainties related to the reference channels and of the γ reconstruction and obtain

$$\frac{\mathcal{B}(f_0(1710) \rightarrow \pi\pi)}{\mathcal{B}(f_0(1710) \rightarrow K\bar{K})} = 0.64 \pm 0.27_{\text{stat}} \pm 0.18_{\text{sys}}, \quad (12)$$

in agreement with the world average value of $0.41^{+0.11}_{-0.17}$ [18].

3 Dalitz plot analysis of η_c three-body decays

The results presented here are based on the full data set collected with the BaBar detector using an integrated luminosity of 519 fb^{-1} recorded at center-of-mass energies at and near the $\Upsilon(nS)$ ($n = 2, 3, 4$) resonances. In the present analysis, we consider the three-body η_c decays to $\eta' K^+ K^-$, $\eta' \pi^+ \pi^-$, and $\eta \pi^+ \pi^-$, using two-photon interactions, $e^+ e^- \rightarrow e^+ e^- \gamma^* \gamma^* \rightarrow e^+ e^- \eta_c$, where γ^* indicate the intermediate quasi-real virtual photons.

3.1 Study of $\gamma\gamma \rightarrow \eta' h^+ h^-$ and $\gamma\gamma \rightarrow \eta \pi^+ \pi^-$

We first study the reactions

$$\gamma\gamma \rightarrow \eta' h^+ h^-, \quad (13)$$

where $h^+ h^-$ indicates a $\pi^+ \pi^-$ or $K^+ K^-$ system. The η' is reconstructed in the two decay modes $\eta' \rightarrow \rho^0 \gamma$, $\rho^0 \rightarrow \pi^+ \pi^-$, and $\eta' \rightarrow \eta \pi^+ \pi^-$, $\eta \rightarrow \gamma\gamma$. We define p_T as the magnitude of the

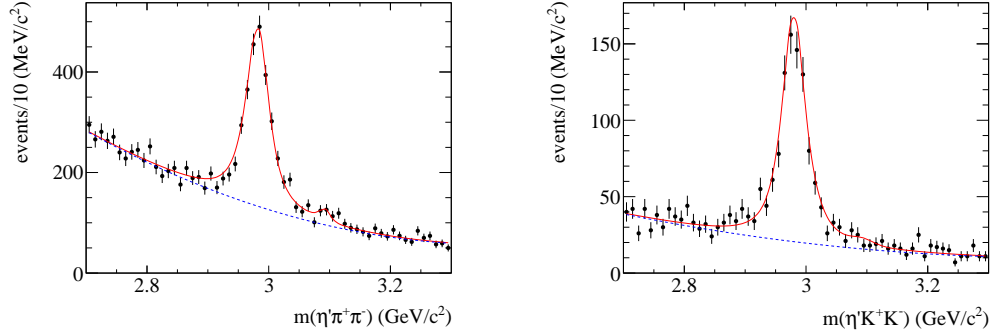


Figure 5: Invariant-mass distributions of selected (Left) $\eta'\pi^+\pi^-$ and (Right) $\eta'K^+K^-$ candidates summed over the $\eta' \rightarrow \rho^0\gamma$ and $\eta' \rightarrow \eta\pi^+\pi^-$ decay modes.

transverse momentum of the $\eta'h^+h^-$ system, in the e^+e^- rest frame, with respect to the beam axis. Well reconstructed two-photon events with quasi-real photons are expected to have low values of p_T . For the selection of the $\eta'\pi^+\pi^-$ final state, we require all four charged tracks to be positively identified as pions. For the $\eta'K^+K^-$ final state, we require the two charged tracks assigned to the η' decay to be positively identified as pions and the other two to be positively identified as kaons. We require $p_T < 0.05$ GeV/c and $p_T < 0.15$ GeV/c, for the $\eta' \rightarrow \rho^0\gamma$ and $\eta' \rightarrow \eta\pi^+\pi^-$, respectively. We discriminate against Initial State Radiation (ISR) events $e^+e^- \rightarrow \gamma_{ISR}h^+h^-$, by requiring the recoil mass $M_{\text{rec}} \equiv (p_{e^+e^-} - p_{\text{rec}})^2 > 2$ GeV²/c⁴, where $p_{e^+e^-}$ is the four-momentum of the initial state e^+e^- and p_{rec} is the reconstructed four-momentum of the candidate $\eta'(\eta)h^+h^-$ system.

The $\eta'\pi^+\pi^-$ and $\eta'K^+K^-$ mass spectra, summed over the $\eta' \rightarrow \rho^0\gamma$ and $\eta' \rightarrow \eta\pi^+\pi^-$ decay modes are shown in fig. 5, where prominent η_c signals can be observed. In particular, fig. 5(Right) reports the first observation of the decay $\eta_c \rightarrow \eta'K^+K^-$.

We also study the reaction

$$\gamma\gamma \rightarrow \eta\pi^+\pi^-, \quad (14)$$

where $\eta \rightarrow \gamma\gamma$ and $\eta \rightarrow \pi^+\pi^-\pi^0$. In this case the two-photon reaction is selected by requiring $p_T < 0.1$ GeV/c for both η decay modes. The corresponding $\eta\pi^+\pi^-$ mass spectra are shown in fig. 6, where prominent η_c signals can be observed.

To compute the reconstruction and selection efficiency, MC signal events are generated using a detailed detector simulation in which the η_c mesons decay uniformly in phase space. These simulated events are reconstructed and analyzed in the same manner as data. We define the helicity angle θ_H as the angle formed by the h^+ (where $h = \pi, K$), in the h^+h^- rest frame, and the η' (η) direction in the $h^+h^-\eta'$ ($h^+h^-\eta$) rest frame. To smoothen statistical fluctuations, the efficiency maps are parameterized using Legendre polynomials up to $L = 12$ as functions of $\cos\theta_H$ in intervals of $m(h^+h^-)$ and then interpolated linearly between adjacent mass intervals.

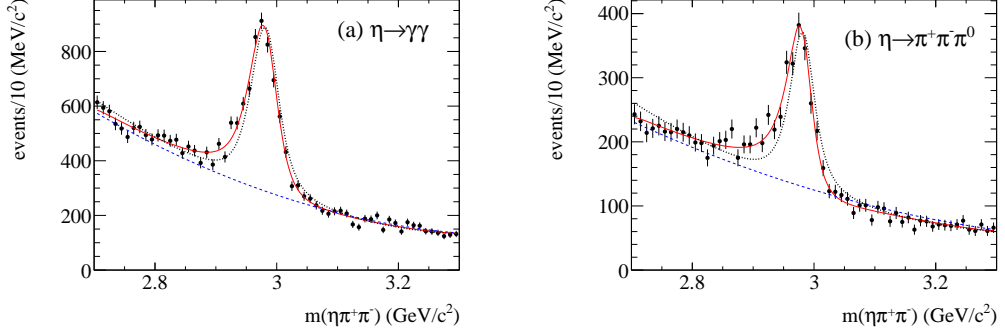


Figure 6: Invariant-mass spectra for selected $\eta\pi^+\pi^-$ candidate events with (a) $\eta \rightarrow \gamma\gamma$ and (b) $\eta \rightarrow \pi^+\pi^-\pi^0$. The solid (red) lines represent the fits including interference described in the text. The dashed (blue) line represents the fitted non-resonant components. The dotted lines represent the fits without interference.

3.2 Yields and branching fractions

We fit the invariant-mass distributions to obtain the numbers of selected η_c events, $N_{\eta'K^+K^-}$, $N_{\eta'\pi^+\pi^-}$, and $N_{\eta\pi^+\pi^-}$, for each η' or η decay mode. We then use the $\eta'K^+K^-$ and $\eta'\pi^+\pi^-$ yields to compute the ratio of branching fractions for η_c to the $\eta'K^+K^-$ and $\eta'\pi^+\pi^-$ final states. This ratio is computed as

$$\mathcal{R} = \frac{\mathcal{B}(\eta_c \rightarrow \eta'K^+K^-)}{\mathcal{B}(\eta_c \rightarrow \eta'\pi^+\pi^-)} = \frac{N_{\eta'K^+K^-}}{N_{\eta'\pi^+\pi^-}} \frac{\epsilon_{\eta'\pi^+\pi^-}}{\epsilon_{\eta'K^+K^-}} \quad (15)$$

for each η' decay mode, where $\epsilon_{\eta'K^+K^-}$ and $\epsilon_{\eta'\pi^+\pi^-}$ are the corresponding efficiencies. We determine $N_{K^+K^-\eta'}$ and $N_{\pi^+\pi^-\eta'}$ from η_c decays by performing binned χ^2 fits to the $\eta'K^+K^-$ and $\eta'\pi^+\pi^-$ invariant-mass spectra, in the 2.7-3.3 GeV/c^2 mass region, separately for the two η' decay modes. In these fits, the η_c signal contribution is described by a simple Breit-Wigner (BW) function convolved with a fixed resolution function (described by the sum of a Gaussian and Crystal Ball functions), with η_c parameters fixed to PDG values [22]. An additional BW function is used to describe the residual background from ISR J/ψ events, and the remaining background is parameterized by a 2nd order polynomial. The fitted $\eta'h^+h^-$ invariant-mass spectra are shown in Fig. 5 summed over the two η' decay modes.

We estimate $\epsilon_{\eta'K^+K^-}$ and $\epsilon_{\eta'\pi^+\pi^-}$ for the η_c signals using the 2-D efficiency functions described above. Each event is first weighted by $1/\epsilon(m, \cos\theta_H)$. Since the backgrounds below the η_c signals have different distributions in the Dalitz plot, we perform a sideband subtraction by assigning an additional weight of +1 to events in the η_c signal region, defined as the (2.93-3.03) GeV/c^2 mass region, and a weight -1 to events in the sideband regions, (2.77-2.87) GeV/c^2 and (3.09-3.19) GeV/c^2 . The two evaluations of the branching fractions, for the two η' decay mode, are in good agreement and give an average value of

$$\frac{\mathcal{B}(\eta_c \rightarrow \eta'K^+K^-)}{\mathcal{B}(\eta_c \rightarrow \eta'\pi^+\pi^-)} = 0.644 \pm 0.039_{\text{stat}} \pm 0.032_{\text{sys}} \quad (16)$$

For the decay $\eta_c \rightarrow \eta\pi^+\pi^-$ the fits without interference do not describe the data well for either η

decay mode. Leaving free the η_c parameters, the fits return masses shifted down by ≈ 10 MeV/ c^2 with respect to PDG averages.

We test the possibility of interference effects of the η_c with each non-resonant two-photon process [23], modifying the fitting function by defining

$$f(m) = |A_{\text{nres}}|^2 + |A_{\eta_c}|^2 + c \cdot 2\text{Re}(A_{\text{nres}}A_{\eta_c}^*), \quad (17)$$

where A_{nres} is the non-resonant amplitude with $|A_{\text{nres}}|^2$ described by a 2^{nd} order polynomial; the coherence factor c is the fraction of the non-resonant events that are true two-photon production of the same final state; the resonant contribution is described by $A_{\eta_c} = \alpha \cdot BW(m) \cdot \exp(i\phi)$, where $BW(m)$ is a simple Breit-Wigner with parameters fixed to PDG values; and α , ϕ , and c are free parameters. The fitted invariant-mass spectra are shown in Fig. 6, where reasonable descriptions of the data are evident. As a comparison we also show the fit the two mass spectra with no interference and fixed η_c parameters and obtain the dotted lines distributions shown in Fig. 6.

3.3 Dalitz plot analysis

We perform Dalitz plot analyses of the $\eta'\pi^+\pi^-$, $\eta'K^+K^-$, and $\eta\pi^+\pi^-$ systems in the η_c mass region using unbinned maximum likelihood fits. Amplitudes are parameterized as described in Ref. [24]. They include a relativistic Breit-Wigner function having a variable width modulated by the Blatt-Weisskopf [25] spin form factors and the relevant spin-angular information. We first fit the two η_c sidebands separately, using an incoherent sum of amplitudes. To model the background composition in the η_c signal region, we take a weighted average of the two fitted fractional contributions, and normalize using the results from the fit to the η_c signal region.

3.3.1 Dalitz plot analysis of $\eta_c \rightarrow \eta'K^+K^-$.

Figure 7(a) shows the Dalitz plot for the selected $\eta_c \rightarrow \eta'K^+K^-$ candidates in the data, for the two η' decay modes combined (930 events). We observe that this η_c decay mode is dominated by a diagonal band on the low mass side of the Dalitz plot. The $m(K^+K^-)$ spectrum shows a large structure in the region of the $f_0(1710)$ resonance. The combined $m(\eta'K^\pm)$ invariant-mass spectrum shows a structure at threshold due to the $K_0^*(1430)$ accompanied by weaker resonant structures. The $K_0^*(1430)$ is a relatively broad resonance decaying to $K\pi$, $K\eta$, and $K\eta'$. The measured $K\eta$ relative branching fraction is $\frac{\mathcal{B}(K_0^*(1430) \rightarrow K\eta)}{\mathcal{B}(K_0^*(1430) \rightarrow K\pi)} = 0.092 \pm 0.025^{+0.010}_{-0.025}$ [26], while the $K\eta'$ has only been observed in Ref. [27]. To describe the $K_0^*(1430)$ lineshape in the $K\eta'$ projection, we model it using a simplified coupled-channel Breit-Wigner function, which ignores the small $K\eta$ contribution. We parameterize the $K_0^*(1430)$ signal as

$$BW(m) = \frac{1}{m_0^2 - m^2 - i(\rho_1(m)g_{K\pi}^2 + \rho_2(m)g_{K\eta'}^2)}, \quad (18)$$

where m_0 is the resonance mass, $g_{K\pi}$ and $g_{K\eta'}$ are the couplings to the $K\pi$ and $K\eta'$ final states, and $\rho_j(m) = 2P/m$ are the respective Lorentz-invariant phase-space factors, with P the decay particle momentum in the $K_0^*(1430)$ rest frame. The values of m_0 and the g_{K_j} couplings cannot

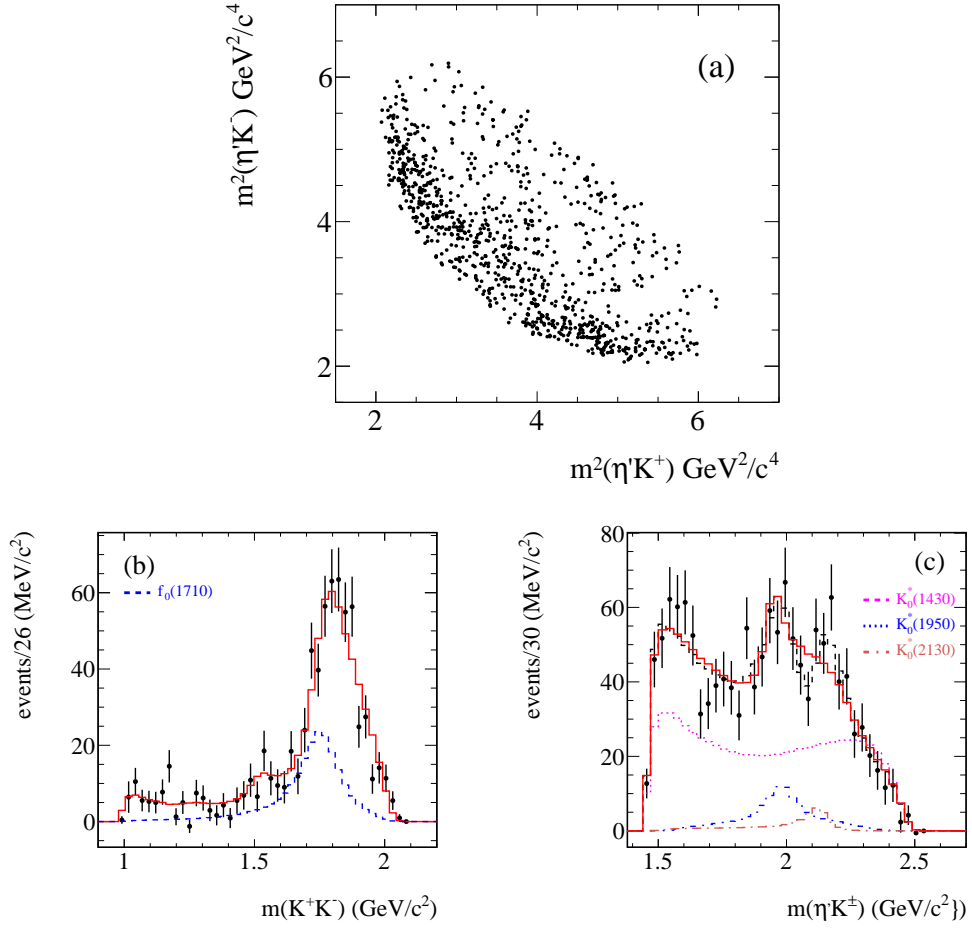


Figure 7: (a) Dalitz plot for selected $\eta_c \rightarrow \eta' K^+ K^-$ candidates in the η_c signal region, summed over the two η' decay modes. Linear-scale mass projections (b) $m(K^+ K^-)$ and (c) $m(\eta' K^\pm)$, after subtraction of the background. The solid (red) histograms represent the results of the fit described in the text. The (black) dashed line in (c) shows the solution which include the presence of $K_0^*(2130)$. The other histograms display the contributions from each of the listed components.

be derived from the $K\eta'$ system only, and therefore we make use of the $K\pi$ S -wave measurement from BaBar [28]. We average the reported quasi model-independent (QMI) measurements of the $K\pi$ S -wave from $\eta_c \rightarrow K_s^0 K\pi$ and $\eta_c \rightarrow K^+ K^- \pi^0$ decays, and obtain the modulus squared of the amplitude and the phase shown in Fig. 8.

We perform a simultaneous binned χ^2 fit to the $K\pi$ S -wave amplitude and phase from threshold up to $1.72 \text{ GeV}/c^2$. We model the $K\pi$ S -wave in this region as $S\text{-wave}(m) = B(m) + c \cdot BW_{K\pi}(m)e^{i\phi}$, where $BW_{K\pi}(m)$ is given by Eq.(18), $B(m)$ is an empirical background term, parameterized as $B(m) = \rho_1(m)e^{-\alpha m}$, and c , ϕ , and α are free parameters. The results of the fit are shown in Fig. 8 as the solid (red) lines.

We perform a Dalitz plot analysis of the $\eta_c \rightarrow \eta' K^+ K^-$ decay channel by using the $\eta' f_0(1710)$

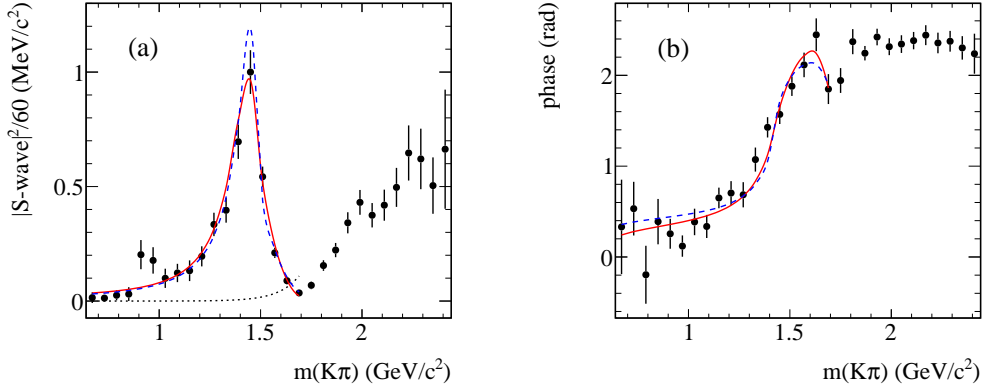


Figure 8: The (a) squared modulus and (b) phase of the $K\pi$ S -wave averaged over the $\eta_c \rightarrow K_S^0 K\pi$ and $\eta_c \rightarrow K^+ K^- \pi^0$ from the BaBar [28] QMI analysis. The full (red) lines represent the result from the fit with free $g_{K\eta'}$ and $g_{K\pi}^2$ parameters. The dashed (blue) lines represent the result from the fit with a fixed $g_{K\eta'}^2/g_{K\pi}^2$ ratio [12]. The dotted (black) line in (a) represents the empirical background contribution.

intermediate state as the reference amplitude. The projections of the fit result are shown in Fig. 7(b)-(c), along with the largest signal components. We measure the $f_0(1710)$ parameters, listed in Table 3. We also measure the parameters of the $K_0^*(1950)$ (see Table 3) for which there is only one previous measurement from the LASS collaboration [29]. For the $K_0^*(1430)$ resonance we make use of an iterative procedure, combining the results of the present Dalitz plot analysis with previous measurements (see ref. [12] for details). The results from the Dalitz analysis are given in Table 4.

An inspection of Fig. 7(c) suggests an additional enhancement in the $m(\eta' K^\pm)$ around a mass of ≈ 2100 MeV/ c^2 . We explore this possibility adding, in the Dalitz plot analysis, an additional scalar resonance in this mass region with free parameters. The presence of this additional resonance also affects the parameters of the $K_0^*(1950)$ which are also left free in the fit. The results from this solution are listed in Table 4, labelled as solution (b). A comparison between the two fits on the $m(\eta' K^\pm)$ projection is shown in Fig. 7(c). However, an application of the Wilks theorem for the individual significances of the $K_0^*(1950)$ and $K_0^*(2130)$ in this new fit, obtain values of 4.3σ and 2.7σ , respectively. Since the local significance of the $K_0^*(2130)$ is less than 3σ , we do not consider the presence of this contribution in the reference fit.

3.3.2 Dalitz plot analysis of $\eta_c \rightarrow \eta' \pi^+ \pi^-$.

Figure 9(a) shows the Dalitz plot for the selected $\eta_c \rightarrow \eta' \pi^+ \pi^-$ candidates in the data, in the η_c signal region, for the two η' decay modes combined (3122 events), and Figs. 9(b)-(c) show the two background subtracted projections in linear mass scale. We observe several diagonal bands in the Dalitz plot, in particular at the lower-left edge. There are corresponding structures in the $m(\pi^+ \pi^-)$ spectrum, including peaks attributable to the $f_0(980)$ and $f_2(1270)$ resonances, and a large structure at high $\pi^+ \pi^-$ mass. A candidate for the large structure in the high $\pi^+ \pi^-$ mass region

Table 3: Resonance parameters from the Dalitz plot analyses of $\eta_c \rightarrow \eta' K^+ K^-$, $\eta_c \rightarrow \eta' \pi^+ \pi^-$, and $\eta_c \rightarrow \eta \pi^+ \pi^-$. Significances are computed using the Wilks theorem [30] and do not include systematic uncertainties.

Resonance	Mass (MeV/ c^2)	$g_{K\pi}^2$ (GeV $^2/c^4$)	$g_{K\eta'}^2$ (GeV $^2/c^4$)
$\eta_c \rightarrow \eta' K^+ K^-$			
$K_0^*(1430)$			
$\eta_c \rightarrow K \bar{K} \pi$	1447 ± 8	0.414 ± 0.026	0.197 ± 0.105
fixed $\frac{g_{\eta'K}^2}{g_{\pi K}^2}$	1453 ± 22	0.462 ± 0.036	
Resonance	Mass (MeV/ c^2)	Γ (MeV)	significance ($n\sigma$)
$f_0(1710)$	$1757 \pm 24 \pm 9$	$175 \pm 23 \pm 4$	11.4
(a) $K_0^*(1950)$	$1942 \pm 22 \pm 5$	$80 \pm 32 \pm 20$	3.3
(b) $K_0^*(1950)$	$1979 \pm 26 \pm 3$	$144 \pm 44 \pm 21$	4.3
$K_0^*(2130)$	$2128 \pm 31 \pm 9$	$95 \pm 42 \pm 76$	2.7
$\eta_c \rightarrow \eta' \pi^+ \pi^-$			
$f_0(500)$	953 ± 90	335 ± 81	
$f_2(1430)$	$1440 \pm 11 \pm 3$	$46 \pm 15 \pm 5$	4.4
$f_0(2100)$	$2116 \pm 27 \pm 17$	$289 \pm 34 \pm 15$	10
$\eta_c \rightarrow \eta \pi^+ \pi^-$			
$a_0(1700)$	$1704 \pm 5 \pm 2$	$110 \pm 15 \pm 11$	8

Table 4: Fractions and relative phases from the Dalitz plot analysis of $\eta_c \rightarrow \eta' K^+ K^-$.

Intermediate state	fraction (%)	phase (rad)
$f_0(1710)\eta'$	$29.5 \pm 4.7 \pm 1.6$	0.
$K_0^*(1430)^+ K^-$	$53.9 \pm 7.2 \pm 2.0$	$0.61 \pm 0.13 \pm 0.45$
$K_0^*(1950)^+ K^-$	$2.4 \pm 1.2 \pm 0.4$	$0.46 \pm 0.29 \pm 0.50$
$f_0(1500)\eta'$	$0.8 \pm 1.0 \pm 0.3$	$0.32 \pm 0.54 \pm 0.10$
$f_0(980)\eta'$	$4.7 \pm 2.7 \pm 0.4$	$-0.74 \pm 0.55 \pm 0.05$
$f_2(1270)\eta'$	$2.9 \pm 1.5 \pm 0.11$	$2.9 \pm 0.38 \pm 0.09$
sum	$94.3 \pm 9.3 \pm 2.6$	
p -value	18%	

is the $f_0(2100)$ resonance, observed in radiative J/ψ decay to $\gamma\eta\eta$ [7]. We take $f_0(2100)\eta'$ as the reference contribution, and perform a Dalitz plot analysis whose results are given in Table 5. We leave free the $f_0(2100)$ resonance parameters and obtain the values reported in Table 4 with a significance of 10σ . To describe the small enhancement around $1.43 \text{ GeV}/c^2$, we test both spin-2 and spin-0 hypotheses with free resonance parameters; we obtain $\Delta(-2 \log \mathcal{L}) = 2.4$ in favor of the spin-2 hypothesis, so we attribute this signal to the $f_2(1430)$ resonance, and report the fitted

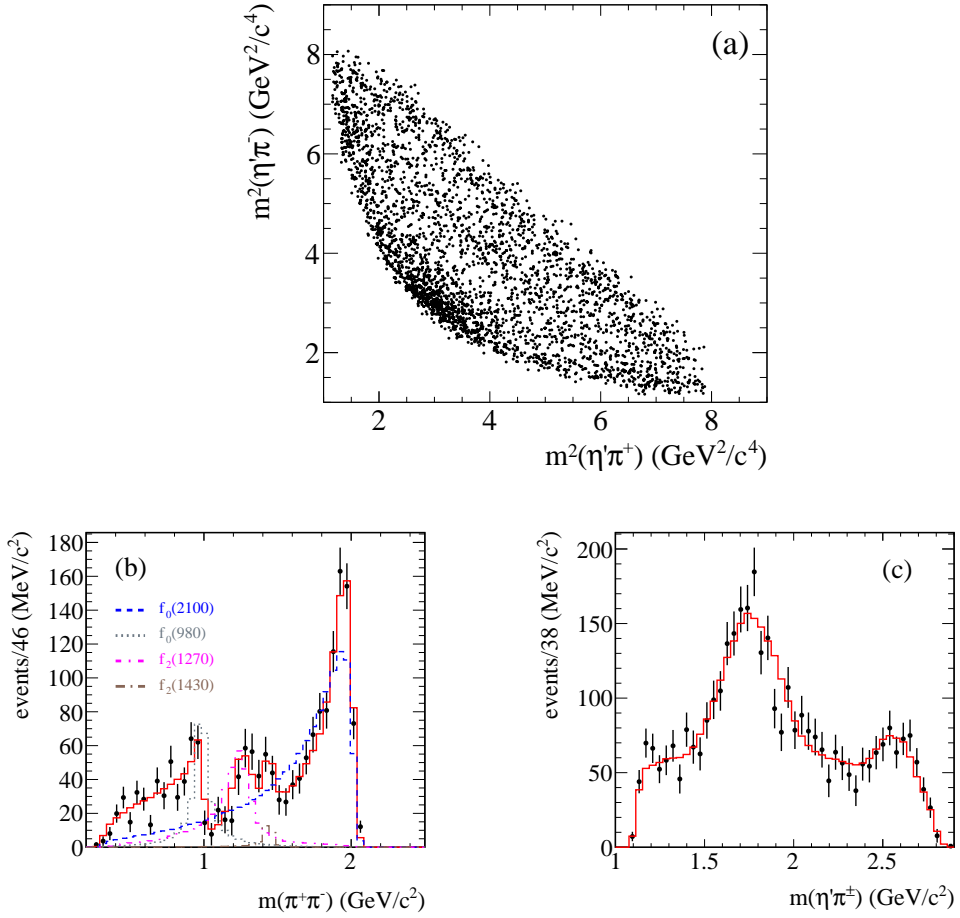


Figure 9: (a) Dalitz plot for selected $\eta_c \rightarrow \eta' \pi^+ \pi^-$ candidates in the η_c signal region, summed over the two η' decay modes. Linear-scale mass projections (b) $m(\pi^+ \pi^-)$ and (c) $m(\eta' \pi^\pm)$, after subtraction of the background. The solid (red) histograms represent the results of the fit described in the text, and the other histograms display the contributions from each of the listed components.

parameter values in Table 4. We test the significance of this signal by removing it from the list of the resonances, obtaining $\Delta(-2 \log \mathcal{L}) = 23.8$ and a significance of 4.4σ .

3.3.3 Dalitz plot analysis of $\eta_c \rightarrow \eta \pi^+ \pi^-$.

Figure 10(a) shows the Dalitz plot for the selected $\eta_c \rightarrow \eta \pi^+ \pi^-$ candidates in the data, in the η_c signal region, for the two η decay modes combined (9303 events), and Figs. 10(b)-(c) show two background subtracted linear-mass projections. We observe that the Dalitz plot is dominated by horizontal and vertical bands due to the $a_0(980)$ and diagonal bands in the $\pi^+ \pi^-$ final state corresponding to $f_0(500)$, $f_0(980)$, and $f_2(1270)$ resonances. We take $a_0(980)^+ \pi^-$ as the reference contribution, and perform a Dalitz plot analysis as described above. The resulting

Table 5: Fractions and relative phases from the Dalitz plot analysis of $\eta_c \rightarrow \eta' \pi^+ \pi^-$.

Intermediate state	fraction (%)	phase (rad)
$f_0(2100)\eta'$	$74.9 \pm 7.5 \pm 3.6$	0.
$f_0(500)\eta'$	$4.3 \pm 2.3 \pm 0.7$	$-5.89 \pm 0.24 \pm 0.10$
$f_0(980)\eta'$	$16.1 \pm 2.4 \pm 0.5$	$-5.31 \pm 0.16 \pm 0.04$
$f_2(1270)\eta'$	$22.1 \pm 2.9 \pm 2.4$	$-3.60 \pm 0.16 \pm 0.03$
$f_2(1430)\eta'$	$1.9 \pm 0.7 \pm 0.1$	$-2.45 \pm 0.32 \pm 0.11$
$a_2(1710)\pi$	$3.2 \pm 1.9 \pm 0.5$	$-0.75 \pm 0.27 \pm 0.11$
$a_0(1950)\pi$	$2.5 \pm 1.1 \pm 0.1$	$-0.02 \pm 0.32 \pm 0.06$
$f_2(1800)\eta'$	$5.3 \pm 2.2 \pm 1.4$	$0.67 \pm 0.24 \pm 0.08$
sum	$130.5 \pm 9.5 \pm 4.7$	
<i>p</i> -value	20%	

Table 6: Fractions and relative phases from the Dalitz plot analysis of $\eta_c \rightarrow \eta \pi^+ \pi^-$. The first errors are statistical, the second systematic.

Intermediate state	fraction (%)	phase (rad)
$a_0(980)^+ \pi^-$	$12.3 \pm 1.2 \pm 2.8$	0.
$a_2(1310)^+ \pi^-$	$2.5 \pm 0.7 \pm 0.9$	$-1.04 \pm 0.13 \pm 0.20$
$f_0(500)\eta$	$4.3 \pm 1.3 \pm 1.1$	$0.54 \pm 0.14 \pm 0.24$
$f_2(1270)\eta$	$4.6 \pm 0.9 \pm 0.8$	$-1.15 \pm 0.11 \pm 0.05$
$f_0(980)\eta$	$5.7 \pm 1.3 \pm 1.5$	$-2.41 \pm 0.09 \pm 0.07$
$f_0(1500)\eta$	$4.2 \pm 0.7 \pm 0.9$	$2.32 \pm 0.13 \pm 0.17$
$a_0(1450)^+ \pi^-$	$15.0 \pm 2.4 \pm 3.2$	$2.60 \pm 0.09 \pm 0.11$
$a_0(1700)^+ \pi^-$	$3.5 \pm 0.8 \pm 0.8$	$1.39 \pm 0.15 \pm 0.20$
$f_2(1950)\eta$	$4.2 \pm 1.0 \pm 1.0$	$-1.59 \pm 0.15 \pm 0.21$
resonant sum	$56.3 \pm 3.7 \pm 10.0$	
<i>NR</i>	$172.7 \pm 8.0 \pm 10.0$	$1.67 \pm 0.07 \pm 0.06$
sum	$229.0 \pm 8.8 \pm 14.1$	
<i>p</i> -value	9.3%	

list of contributions to this η_c decay mode is given in Table 6, together with fitted fractions and relative phases. A new $a_0(1700)$ resonance is observed in the $\eta \pi^\pm$ invariant-mass spectrum, with fitted parameters listed in Table 4. The likelihood change obtained when the resonance is excluded from the fit is $\Delta(-2 \log \mathcal{L}) = 72.3$, corresponding to a significance greater than 8σ . We note the presence of a very large non-resonant scalar contribution, and in Table 6, we list both the sum of resonant contributions and the sum including the non-resonant contribution. This effect could be correlated with the interference of the η_c with the two-photon continuum.

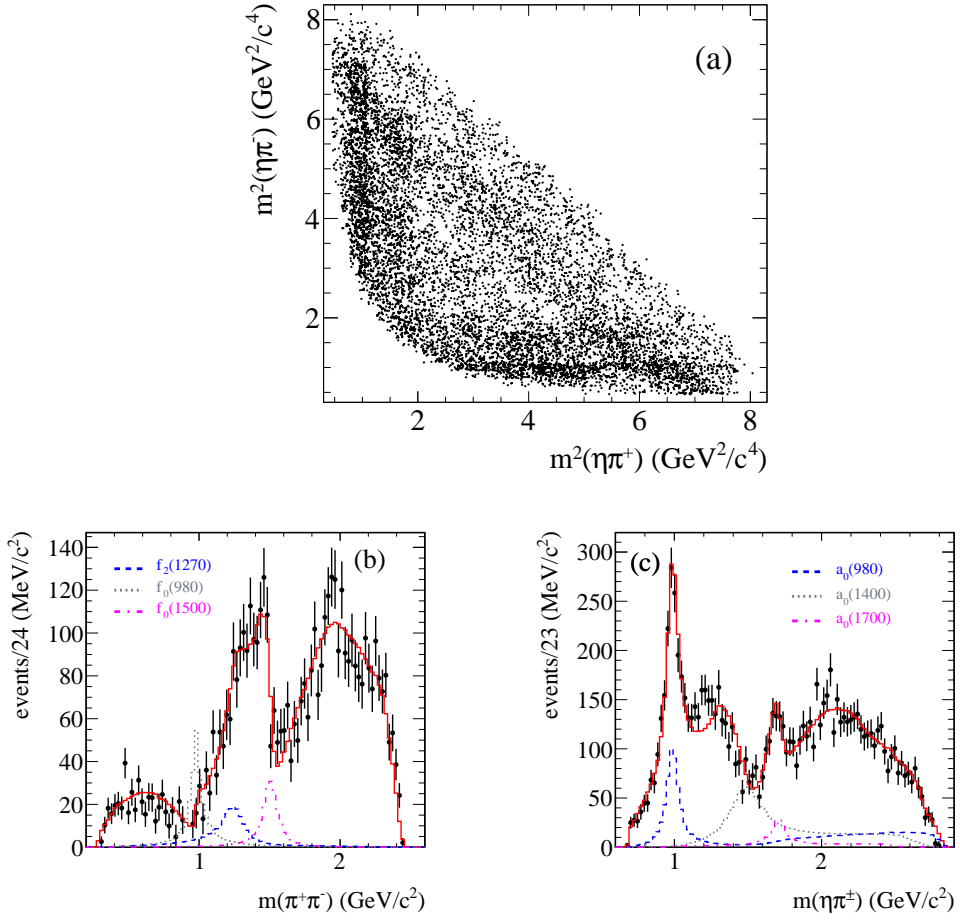


Figure 10: (a) Dalitz plot for selected $\eta_c \rightarrow \eta\pi^+\pi^-$ candidates in the η_c signal region, summed over the two η decay modes. Linear-scale mass projections (b) $m(\pi^+\pi^-)$ and (c) $m(\eta\pi^\pm)$, after subtraction of the background. The solid (red) histograms represent the results of the fit described in the text, and the other histograms display the contributions from each of the listed components.

3.3.4 Results from the $\eta_c \rightarrow \eta K^+ K^-$ analysis.

To complete the list of the results summarized in the present review, we also include in fig. 11(Left), the $\eta_c \rightarrow \eta K^+ K^-$ mass spectrum combined for the $\eta \rightarrow \gamma\gamma$ and $\eta \rightarrow \pi^+\pi^-\pi^0$ decay modes, first observed by BaBar [26].

Figure. 11(Right) shows the squared $K^+ K^-$ mass projection from the η_c Dalitz plot, where signals of $f_0(1500)$ and $f_0(1710)$ can be seen. The Dalitz plot analysis allow to measure the fractions relative to these resonant contributions which are listed in Table 7.

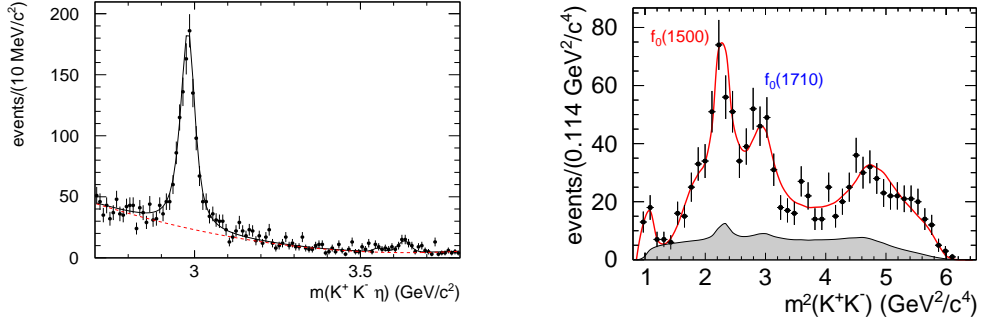


Figure 11: (Left) Invariant $\eta K^+ K^-$ mass spectrum from $\gamma\gamma \rightarrow \eta K^+ K^-$. (Right) Squared $K^+ K^-$ mass projection from the η_c Dalitz plot. The line is the result from the Dalitz plot analysis.

Table 7: Fractional contributions to $\eta_c \rightarrow \eta h^+ h^-$ and $\eta_c \rightarrow \eta' h^+ h^-$ decays of selected scalar mesons, uncorrected for unseen decay modes.

Final state	$f_0(1500)(\%)$	$f_0(1710)(\%)$	$f_0(2100)(\%)$
$\eta K^+ K^-$	$23.7 \pm 7.0 \pm 1.8$	$8.9 \pm 0.2 \pm 0.4$	
$\eta \pi^+ \pi^-$	$4.2 \pm 0.7 \pm 0.9$		0.
$\eta' K^+ K^-$	$0.8 \pm 1.0 \pm 0.3$	$29.5 \pm 4.7 \pm 1.6$	
$\eta' \pi^+ \pi^-$	0.3 ± 0.2		$74.9 \pm 7.5 \pm 3.5$

4 Conclusions

The study of radiative $\Upsilon(1S)$ decay to $\gamma\pi^+\pi^-$ and γK^+K^- shows the presence of the gluonium candidates $f_0(1500)$ and $f_0(1710)$, in agreement with what observed in J/ψ radiative decays.

In the framework of the identification of scalar gluonium states, it is interesting to compare the rates of η_c decays into a gluonium candidate state and an η or an η' meson.

Table 7 summarizes relevant results from the analyses reported in the present review. We observe an enhanced contribution of $f_0(1710)$ in η_c decays to η' and an enhanced contribution of $f_0(1500)$ in η_c decays to η . This effect may point to an enhanced gluonium content in the $f_0(1710)$ meson. A similar effect is observed for the $f_0(2100)$ resonance. The observation of $f_0(2100)$ in both J/ψ radiative decays and in $\eta_c \rightarrow \eta' \pi^+ \pi^-$ allows to add this state in the list of the candidates for the scalar glueball.

References

- [1] Y. Chen, *et al.* Phys. Rev. D **73**, 014516 (2006) [arXiv:hep-lat/0510074].
- [2] P. Minkowski and W. Ochs, Eur. Phys. J. C **9** (1999), 283-312 [arXiv:hep-ph/9811518].

- [3] C. Amsler and F. E. Close, Phys. Lett. B **353** (1995), 385-390 [arXiv:hep-ph/9505219].
- [4] C. Amsler and F. E. Close, Phys. Rev. D **53** (1996), 295-311 [arXiv:hep-ph/9507326].
- [5] S. Janowski, F. Giacosa and D. H. Rischke, Phys. Rev. D **90** (2014) no.11, 114005 [arXiv:1408.4921 [hep-ph]].
- [6] L. C. Gui *et al.* [CLQCD Collaboration], Phys. Rev. Lett. **110** (2013) no.2, 021601 [arXiv:1206.0125 [hep-lat]].
- [7] M. Ablikim *et al.* [BESIII Collaboration], Phys. Rev. D **87** (2013) no.9, 092009 [erratum: Phys. Rev. D **87** (2013) no.11, 119901] [arXiv:1301.0053 [hep-ex]].
- [8] L. Kopke and N. Wermes, Phys. Rept. **174** (1989), 67.
- [9] S. Dobbs, A. Tomaradze, T. Xiao and K. K. Seth, Phys. Rev. D **91** (2015) no.5, 052006 [arXiv:1502.01686 [hep-ex]].
- [10] J. P. Lees *et al.* [BaBar Collaboration], Phys. Rev. D **97** (2018) no.11, 112006 [arXiv:1804.04044 [hep-ex]].
- [11] S. B. Athar *et al.* [CLEO Collaboration], Phys. Rev. D **73** (2006), 032001 [arXiv:hep-ex/0510015].
- [12] J. P. Lees *et al.* [BaBar Collaboration], Phys. Rev. D **104** (2021) no.7, 072002 [arXiv:2106.05157 [hep-ex]].
- [13] C. N. Yang, Phys. Rev. **77** (1950), 242-245.
- [14] L. A. Harland-Lang, V. A. Khoze, M. G. Ryskin and W. J. Stirling, Eur. Phys. J. C **73** (2013), 2429 [arXiv:1302.2004 [hep-ph]].
- [15] S. D. Bass and P. Moskal, Rev. Mod. Phys. **91** (2019) no.1, 015003 [arXiv:1810.12290 [hep-ph]].
- [16] S. M. Flatte, Phys. Lett. B **63** (1976), 224-227.
- [17] T. A. Armstrong *et al.* [WA76 Collaboration], Z. Phys. C **51** (1991), 351-364.
- [18] C. Patrignani *et al.* (Particle Data Group), Chin. Phys. C **40**, 100001 (2016).
- [19] J. Becker *et al.* [Mark-III Collaboration], Phys. Rev. D **35** (1987), 2077.
- [20] J. P. Lees *et al.* [BaBar Collaboration], Phys. Rev. D **85** (2012), 112010 [arXiv:1201.5897 [hep-ex]].
- [21] A. J. Bevan *et al.* [BaBar and Belle Collaborations], Eur. Phys. J. C **74** (2014), 3026 [arXiv:1406.6311 [hep-ex]].

- [22] P.A. Zyla *et al.* (Particle Data Group), Prog. Theor. Exp. Phys. 2020, 083C01 (2020).
- [23] C. C. Zhang *et al.* [Belle Collaboration], Phys. Rev. D **86** (2012), 052002 [arXiv:1206.5087 [hep-ex]].
- [24] D. Asner, [arXiv:hep-ex/0410014].
- [25] J. M. Blatt and V. F. Weisskopf, Springer, 1952, ISBN 978-0-471-08019-0.
- [26] J. P. Lees *et al.* [BaBar Collaboration], Phys. Rev. D **89** (2014) no.11, 112004 [arXiv:1403.7051 [hep-ex]].
- [27] M. Ablikim *et al.* [BESIII Collaboration], Phys. Rev. D **89** (2014) no.7, 074030 [arXiv:1402.2023 [hep-ex]].
- [28] J. P. Lees *et al.* [BaBar Collaboration], Phys. Rev. D **93** (2016), 012005 [arXiv:1511.02310 [hep-ex]].
- [29] D. Aston, *et al.* [LASS Collaboration] Nucl. Phys. B **296** (1988), 493-526.
- [30] S. S. Wilks, Ann. Math. Stat. 9 (1938) 60.